MAGNETIC FIELD CALCULATION IN PERMANENT MAGNET MOTORS WITH ROTOR ECCENTRICITY : WITH SLOTTING EFFECT CONSIDERED

Ungtae Kim and Dennis K. Lieu

Electro-Mechanical Design Laboratory

Department of Mechanical Engineering

University of California

Berkeley, CA 94720

ABSTRACT

An analytical technique has been developed to predict the instantaneous magnetic field distribution in the air gap of a permanent magnet motor. The effect of the stator slotting and the rotor eccentricity on the magnetic field has been considered. The slotting effect is explained by a newly redefined boundary value problem in polar coordinates in the annular air gap/magnet region of a multi-pole permanent magnet motor. A perturbation technique is introduced to describe the effect of the rotor eccentricity. The analytical method has been validated by a corresponding finite element model. Two prototype motors are used as examples to show the effectiveness of the analytical technique proposed in the paper. The analytical solutions are in good agreement with those obtained by the finite element method, both in amplitude and wave form.

INTRODUCTION

Magnetic field analysis in a brushless permanent magnet motor is an important prerequisite for the prediction of back-emf waveform, cogging torque, and force. Specially, accurate knowledge of the flux density distribution in the air gap is essential for the accurate prediction of the motor performance. Magnet configuration, magnetization direction, air gap length, and the number of the pole and slot combination have significant effects on the flux density distribution in the air gap.

Most brushless motors in disk drive spindles have slotted stators which not only reduce the total flux per pole but change the flux waveform. The effects of slotting on the air gap field have been explained by introducing permeance functions obtained by conformal mappings for geometrically simplified slot models [1][2]. The real air gap flux density is then calculated by multiplying the flux density calculated from the slotless stator model by the relative permeance function. However, this calculation method can give the flux density distribution only at the stator outer surface because the permeance function is obtained from one-dimensional field theory assuming that the flux density varies only with the circumferential coordinate and depends on the angle of rotation of the rotor. This assumption may be appropriate to induction motors in which the air gap length is small. In a permanent magnet motor which has a relatively larger effective air gap length due to the existence of permanent magnets, one-dimensional permeance functions may result in a poor prediction and hence may need two-dimmensional permeance functions as proposed by Zhu [2]. The two dimensional permeance function proposed by Zhu et al, can give the flux density at any position inside the air gap but is a nonlinear function of position, which makes it impossible to analytically integrate the field variables for further

calculations. Unbalanced magnetic force and cogging torque are usually calculated by the Maxwell stress tensor method which integrates the magnetically induced stresses around any closed loop inside the air gap, typically in the middle of the air gap between the rotor and the stator. Accordingly, their calculations can only be executed by a numerical method if a conventional permeance function is used. Another disadvantage of using the conventional permeance functions, regardless of whether they are one- or two-dimensional, is that they can not be used to calculate the circumferential flux density distribution which is necessary for cogging torque calculation by the Maxwell stress tensor method.

The present paper explains a new analytical method to calculate the magnetic field in the air gap region affected by the stator slots. The analysis is based on a two-dimensional magnetic field theory in polar coordinates with an emphasis on slotting effects in the flux density distribution. The present paper is a direct extension of the authors' previous paper [3]. Hence, the rotor eccentric effects are considered. The analysis starts with calculating the radial flux density along the outer surface of a smooth stator. The real flux density of the radial direction at the outer surface of the slot is calculated from multiplication of a relative permeance function and is regarded as a new boundary condition. Then, a new boundary value problem is set up with modified boundary conditions. This analysis produces more satisfying solutions than a similar one reported by Liu et al in [4] and is easier to apply to the calculation of the magnetic field caused by rotor eccentricity. The magnetic field solutions obtained by this analysis can be easily utilized for analytical expressions for unbalanced magnetic pull and cogging torque. As examples, permanent magnet motors with an external rotor were chosen to verify the analytical method

proposed in the present paper. The results are verified by those of finite element analyses. While finite element methods provide an accurate means to determine the flux density distribution in a motor, they are usually time-consuming and do not give enough insight as compared with analytical solutions.

MAGNETIC FIELD CALCULATION WITHOUT ROTOR ECCENTRICITY

Magnetic Field Equation

In this section, an analytical model in two dimension is described for the magnetic field calculation in a permanent magnet motor. The effects of the stator slots on the field are considered. A geometric model of an 8 pole/9 slot brushless permanent magnet DC motor(BLDC PM motor) used in a hard disk drive is described in Fig. 1. Fig. 1(a) shows an original model used for finite element calculation and Fig. 1(b) illustrates its transformed model for analytical calculation. In order to simplify the following analysis; the stator and the rotor back iron is assumed to have infinite permeability; the saturation effects of the iron are ignored; the stator slots are assumed to be rectangular shaped as shown in Fig. 1(b); and finally, the permanent magnets are assumed to be radially magnetized, isotropic, and are assumed to have a linear demagnetization characteristic.

For regions where there is no conductor source, the total magnetic field $\vec{H}$ can be represented by a scalar potential Φ defined as

$$\vec{H} = -\nabla \Phi \tag{1}$$

Therefore, the governing equations for regions without currents are given

$$\frac{\partial^2 \Phi_1}{\partial \xi^2} + \frac{1}{\xi}\frac{\partial \Phi_1}{\partial \psi} + \frac{1}{\xi^2}\frac{\partial^2 \Phi_1}{\partial \psi^2} = 0 \tag{2}$$

$$\frac{\partial^2 \Phi_2}{\partial \xi^2} + \frac{1}{\xi}\frac{\partial \Phi_2}{\partial \psi} + \frac{1}{\xi^2}\frac{\partial^2 \Phi_2}{\partial \psi^2} = \frac{1}{\mu_r}\frac{M_\xi}{\xi} \tag{3}$$

The field vectors, the flux density, $\vec{B}$ and the field intensity, $\vec{H}$ are coupled by

$$\vec{B}_1 = \mu_0 \vec{H}_1 \tag{4}$$

$$\vec{B}_2 = \mu_m \vec{H}_2 + \mu_0 \vec{M} \tag{5}$$

The permeability of the permanent magnet is expressed by $\mu_m = \mu_0 \mu_r$,where μ_0 is the permeability of air and μ_r is the relative permeability of the magnet. $\vec{M}$ is the residual magnetization vector represented by B_r / μ_0 , where B_r is the remanence. In the paper, the subscripts 1 and 2 designate the air gap and the permanent magnet region, respectively. The magnetization distribution is shown for radial magnetization in Fig. 2 and can be represented by a Fourier series expansion [5].

The boundary condition along the stator outer surface of Fig. 1(b) is defined by

$$\begin{aligned} B_{r,1}(r,\theta)\big|_{r=R_S} &= \left\{ \sum_{n=1,3,5\cdots}^{\infty} B_n \cos\left[np(\theta - \omega t)\right] \right\} \left\{ \sum_{m=0}^{\infty} \lambda_m \cos\left(mq\theta\right) \right\} \\ &= \sum_{n=1,3,5\cdots}^{\infty} \sum_{m=0}^{\infty} \frac{1}{2} B_n \lambda_m \left\{ \cos\left[\left(np+mq\right)\theta - np\omega t\right] + \cos\left[\left(np-mq\right)\theta - np\omega t\right] \right\} \end{aligned} \tag{6}$$

where B_n is the flux density amplitude for the slotless model and is given in [5]. p is the number of the pole pairs and q is the number of the slots. λ_m is the amplitude of the relative permeance function and is given in [1] and [2]. The above boundary condition defines the radial component of the flux density at the outer surface of the stator, which is the multiplication of the flux density distribution of the slotless model and the relative

permeance function. The other boundary conditions are defined by the continuity of the normal flux density and tangential field intensity at the respective boundaries.

$$H_{\theta,2}(r,\theta)\Big|_{r=R_r} = 0 \tag{7}$$

$$B_{r,1}(r,\theta)\Big|_{r=R_m} = B_{r,2}(r,\theta)\Big|_{r=R_m} \tag{8}$$

$$H_{\theta,1}(r,\theta)\Big|_{r=R_m} = H_{\theta,2}(r,\theta)\Big|_{r=R_m} \tag{9}$$

where the magnetic vector quantity *B* and *H* are defined in Eq. (4) and (5).

Magnetic Field Solutions

By considering the boundary conditions in Eq. (6) to (9) and the periodicity of the field, the solutions of the boundary value problem may be proposed as in what follows.

For the air gap region,

$$\begin{aligned}\Phi_1(r,\theta) = &\sum_{n=1,3,5\cdots}^{\infty}\left(A_{1n}^0 r^{np} + B_{1n}^0 r^{-np}\right)\cos\left[np(\theta-\omega t)\right] \\ &+ \sum_{n=1,3,5\cdots}^{\infty}\sum_{m=0}^{\infty}\left(C_{1nm}^0 r^{np+mq} + D_{1nm}^0 r^{-np-mq}\right)\cos\left[(np+mq)\theta - np\omega t\right] \\ &+ \sum_{n=1,3,5\cdots}^{\infty}\sum_{m=0}^{\infty}\left(E_{1nm}^0 r^{np-mq} + F_{1nm}^0 r^{-np+mq}\right)\cos\left[(np-mq)\theta - np\omega t\right]\end{aligned} \tag{10}$$

For the permanent magnet regions

$$\begin{aligned}\Phi_2(r,\theta) = &\sum_{n=1,3,5\cdots}^{\infty}\left(A_{2n}^0 r^{np} + B_{2n}^0 r^{-np}\right)\cos\left[np(\theta-\omega t)\right] \\ &+ \sum_{n=1,3,5\cdots}^{\infty}\sum_{m=0}^{\infty}\left(C_{2nm}^0 r^{np+mq} + D_{2nm}^0 r^{-np-mq}\right)\cos\left[(np+mq)\theta - np\omega t\right] \\ &+ \sum_{n=1,3,5\cdots}^{\infty}\sum_{m=0}^{\infty}\left(E_{2nm}^0 r^{np-mq} + F_{2nm}^0 r^{-np+mq}\right)\cos\left[(np-mq)\theta - np\omega t\right]\end{aligned}$$

$$+\frac{1}{\mu_r}\sum_{n=1,3,5\cdots}^{\infty}\frac{r\cdot M_n}{1-(np)^2}\cos\left[np(\theta-\omega t)\right] \tag{11}$$

The arbitrary constants can then be explicitly determined by the boundary conditions. The flux density distribution only in the air gap region is given in the paper.

For the air gap region, the radial and circumferential components of the flux density distribution are derived by Eq. (1) and (4) as

$$\begin{aligned}B_{r,1}(r,\theta) = &-\mu_0\sum_{n=1,3,5\cdots}^{\infty}(np)\hat{A}_{1n}^{0}\left\{\left(\frac{r}{R_r}\right)^{np-1}-\left(\frac{R_s}{R_r}\right)^{2np}\left(\frac{r}{R_r}\right)^{-np-1}\right\}\cos\left[np(\theta-\omega t)\right]\\ &-\mu_0\sum_{n=1,3,5\cdots}^{\infty}\sum_{m=0}^{\infty}\left\{\hat{C}_{1nm}^{0}\left(\frac{r}{R_r}\right)^{np+mq-1}-\hat{D}_{1nm}^{0}\left(\frac{r}{R_r}\right)^{-np-mq-1}\right\}\cos\left[(np+mq)\theta-np\omega t\right]\\ &-\mu_0\sum_{n=1,3,5\cdots}^{\infty}\sum_{m=0}^{\infty}\left\{\hat{E}_{1nm}^{0}\left(\frac{r}{R_r}\right)^{np-mq-1}-\hat{F}_{1nm}^{0}\left(\frac{r}{R_r}\right)^{-np+mq-1}\right\}\cos\left[(np-mq)\theta-np\omega t\right]\end{aligned} \tag{12}$$

$$\begin{aligned}B_{\theta,1}(r,\theta) = &\mu_0\sum_{n=1,3,5\cdots}^{\infty}(np)\hat{A}_{1n}^{0}\left\{\left(\frac{r}{R_r}\right)^{np-1}+\left(\frac{R_s}{R_r}\right)^{2np}\left(\frac{r}{R_r}\right)^{-np-1}\right\}\sin\left[np(\theta-\omega t)\right]\\ &+\mu_0\sum_{n=1,3,5\cdots}^{\infty}\sum_{m=0}^{\infty}\left\{\hat{C}_{1nm}^{0}\left(\frac{r}{R_r}\right)^{np+mq-1}+\hat{D}_{1nm}^{0}\left(\frac{r}{R_r}\right)^{-np-mq-1}\right\}\sin\left[(np+mq)\theta-np\omega t\right]\\ &+\mu_0\sum_{n=1,3,5\cdots}^{\infty}\sum_{m=0}^{\infty}\left\{\hat{E}_{1nm}^{0}\left(\frac{r}{R_r}\right)^{np-mq-1}+\hat{F}_{1nm}^{0}\left(\frac{r}{R_r}\right)^{-np+mq-1}\right\}\sin\left[(np-mq)\theta-np\omega t\right]\end{aligned} \tag{13}$$

where the arbitrary constants are given in Appendix I. The flux density obtained in this way clearly shows that the magnetic field is composed of both the original flux given by

the slotless model and the additional flux caused by the slotting effects. The effects of the pole-slot number combination and the rotor position appear in the equations.

MAGNETIC FIELD CALCULATION WITH ROTOR ECCENTRICITY

Relative Permeance

In this section, the effort to install the eccentric effects on the air gap field with slots in a permanent magnet motor is explained. The rotor eccentricity is introduced by a perturbation method as in the previous paper[3]. The advantage of using the moving coordinates to solve this particular kind of problem is stated in the previous paper. It reduces the numbers of the asymmetric boundary conditions and so makes the solving procedure much more simplified. In order to do the analysis in the moving coordinate system, the relative permeance function needs to be represented by the moving coordinates. Fig. 3 shows the schematic geometry of the transformed model with the rotor eccentricity.

The reverse coordinate transform can be achieved by the similar way described in the appendix of the previous paper [3]. By using the same notations, the fixed coordinates, r and θ, can be represented by the moving coordinates

$$\theta = \psi + \omega t - \frac{\varepsilon}{\xi}\sin\left(\psi + \omega t - \varphi\right) + O(\varepsilon^2) \tag{14}$$

$$r = \xi + \varepsilon\cos\left(\psi + \omega t - \varphi\right) + O(\varepsilon^2) \tag{15}$$

Then, the relative permeance function can be represented

$$\lambda(\theta) = \sum_{m=0}^{\infty} \lambda_m \cos\left(mq\theta\right)$$

$$= \sum_{m=0}^{\infty} \lambda_m(\xi_s,\psi)\cos\left[mq[\psi+\omega t]-mq\frac{\varepsilon}{\xi}\sin(\psi+\omega t-\varphi)\right]$$

$$\approx \sum_{m=0}^{\infty} \lambda_m \cos[mq(\psi+\omega t)]$$

$$= \lambda(\psi) \qquad (16)$$

Note that the perturbation effects in the phases are neglected for simplicity. Those effects are not believed to be so great compared with the finite element results. Eq. (16) assumes that the relative permeance function is obtained by neglecting the effect of the rotor eccentricity on the air gap shape and hence λ_m does not vary with the coordinates. The real flux density distribution at the outer stator surface can then be obtained by multiplying the flux density of the slotless model by the relative permeance function of the moving coordinates.

The stator outer surface can be described by the moving coordinates as

$$\xi_s = R_s - \varepsilon\cos(\psi+\omega t-\varphi)+O(\varepsilon^2) \qquad (17)$$

where the perturbation quantity $\varepsilon = e \cdot g$, represents the rotor eccentricity magnitude from the stator center and φ gives the rotational position of the rotor eccentricity. Both eccentricity quantities make it possible to express static rotor eccentricity, dynamic rotor eccentricity, or their combination. Then, the radial flux density at ξ_s is derived in a perturbation form by substituting Eq.(17) into the flux density distribution equation for a slotless model with the rotor eccentricity

$$\hat{B}_{\xi,1}(\xi,\psi,\varepsilon)\Big|_{\xi=\xi_s} = -\sum_{n=1,3,5\cdots}^{\infty} 2\mu_0(np)\left(\frac{R_s}{R_r}\right)^{np-1}\hat{B}_n\cos[np\psi]$$

$$-\varepsilon\frac{\mu_0}{R_s}\sum_{n=1,3,5\cdots}^{\infty}\left[np\left(\frac{R_s}{R_r}\right)^{np-1}\hat{B}_n+(np-1)\left\{W_n\left(\frac{R_s}{R_r}\right)^{np-1}-X_n\left(\frac{R_s}{R_r}\right)^{-np+1}\right\}\right]$$

$$\cdot\cos\left[(np-1)\psi-\omega t+\varphi\right]$$

$$-\varepsilon\frac{\mu_0}{R_s}\sum_{n=1,3,5\cdots}^{\infty}\left[np\left(\frac{R_s}{R_r}\right)^{np-1}\hat{B}_n+(np+1)\left\{Y_n\left(\frac{R_s}{R_r}\right)^{np+1}-Z_n\left(\frac{R_s}{R_r}\right)^{-np-1}\right\}\right]$$

$$\cdot\cos\left[(np+1)\psi+\omega t-\varphi\right] \qquad (18)$$

where $\hat{B}_n$ is given in Appendix I and W_n, X_n, Y_n, and Z_n are given in [3].

The real flux density distribution becomes

$$B_{\xi,1}(\xi,\psi,\varepsilon)\Big|_{\xi=\xi_s}=\left\{\hat{B}_{\xi,1}(\xi,\psi)\Big|_{\xi=\xi_s}\right\}\cdot\{\lambda(\psi)\}$$

$$=\sum_{n=1,3,5\cdots}^{\infty}\sum_{m=0}^{\infty}X_{nm}\left\{\cos\left[(np+mq)\psi+mq\omega t\right]\right.$$

$$\left.+\cos\left[(np-mq)\psi-mq\omega t\right]\right\}$$

$$+\varepsilon\sum_{n=1,3,5\cdots}^{\infty}\sum_{m=0}^{\infty}Y_{nm}\left\{\cos\left[(np+mq-1)\psi+(mq-1)\omega t+\varphi\right]\right.$$

$$\left.+\cos\left[(np-mq-1)\psi-(mq+1)\omega t+\varphi\right]\right\}$$

$$+\varepsilon\sum_{n=1,3,5\cdots}^{\infty}\sum_{m=0}^{\infty}Z_{nm}\left\{\cos\left[(np+mq+1)\psi+(mq+1)\omega t-\varphi\right]\right.$$

$$\left.+\cos\left[(np-mq+1)\psi-(mq-1)\omega t-\varphi\right]\right\} \qquad (19)$$

where

$$X_{nm}=-\mu_0\lambda_m np\left(\frac{R_s}{R_r}\right)^{np-1}\hat{B}_n$$

$$Y_{nm} = -\frac{\mu_0 \lambda_m}{2R_s}\left\{np\left(\frac{R_s}{R_r}\right)^{np-1}\hat{B}_n + (np-1)\left(W_n\left(\frac{R_s}{R_r}\right)^{np-1} - X_n\left(\frac{R_s}{R_r}\right)^{-np+1}\right)\right\}$$

$$Z_{nm} = -\frac{\mu_0 \lambda_m}{2R_s}\left\{np\left(\frac{R_s}{R_r}\right)^{np-1}\hat{B}_n + (np+1)\left(Y_n\left(\frac{R_s}{R_r}\right)^{np+1} - Z_n\left(\frac{R_s}{R_r}\right)^{-np-1}\right)\right\}$$

Perturbative Magnetic Field Equation

The magnetic field equation for the eccentric air gap field in a BLDC PM motor has the same form as in the case of the unperturbed field equation if the moving coordinates are used. The only asymmetric boundary condition arises at the outer surface of the stator. Again a perturbation method naturally fits the analysis.

The field equations are given by

$$\frac{\partial^2 \Phi_1}{\partial \xi^2} + \frac{1}{\xi}\frac{\partial \Phi_1}{\partial \psi} + \frac{1}{\xi^2}\frac{\partial^2 \Phi_1}{\partial \psi^2} = 0 \tag{20}$$

$$\frac{\partial^2 \Phi_2}{\partial \xi^2} + \frac{1}{\xi}\frac{\partial \Phi_2}{\partial \psi} + \frac{1}{\xi^2}\frac{\partial^2 \Phi_2}{\partial \psi^2} = \frac{1}{\mu_r}\frac{M_\xi}{\xi} \tag{21}$$

The boundary condition along the stator outer surface is given by Eq. (19) as follows

$$B_{\xi,1}(\xi,\psi)\Big|_{\xi=\xi_s} = -\mu_0 \frac{\partial \Phi_1(\xi,\psi,\varepsilon)}{\partial \xi}\Bigg|_{\xi=\xi_s}$$

$$= \left\{\hat{B}_{\xi,1}(\xi,\psi,\varepsilon)\Big|_{\xi=\xi_s}\right\}\cdot\{\lambda(\psi)\} \tag{22}$$

where $\hat{B}_{\xi,1}(\xi,\psi,\varepsilon)\Big|_{\xi=\xi_s}$ is the flux density distribution of the slotless motor model at the stator outer surface as given in Eq.(18) and $\lambda(\psi)$ is the relative permeance function expressed by the moving coordinates.

The other boundary conditions are identical with the case of the original rotor with no rotor eccentricity.

At $\xi = R_r$,

$$H_{\theta,2}(\xi,\psi,\varepsilon)\Big|_{\xi=R_r} = 0 \tag{23}$$

which results from the infinite permeability of the rotor back iron.

At $\xi = R_m$,

$$B_{\xi,1}(\xi,\psi,\varepsilon)\Big|_{\xi=R_m} = B_{\xi,2}(\xi,\psi,\varepsilon)\Big|_{\xi=R_m} \tag{24}$$

and

$$H_{\psi,1}(\xi,\psi,\varepsilon)\Big|_{\xi=R_m} = H_{\psi,2}(\xi,\psi,\varepsilon)\Big|_{\xi=R_m} \tag{25}$$

These boundary conditions (24) and (25) describe the continuity of the normal flux density and the tangential field intensity flow between the boundary of the air gap and the permanent magnets.

In order to solve the boundary value problem, the following regular perturbation solutions are proposed

$$\Phi_1(\xi,\psi,\varepsilon) = \Phi_1^{(0)}(\xi,\psi) + \varepsilon\Phi_1^{(1)}(\xi,\psi) + \cdots \tag{26}$$

$$\Phi_2(\xi,\psi,\varepsilon) = \Phi_2^{(0)}(\xi,\psi) + \varepsilon\Phi_2^{(1)}(\xi,\psi) + \cdots \tag{27}$$

The magnetic field intensity is then represented by

$$H_i(\xi,\psi,\varepsilon) = -\nabla\Phi_i^{(0)}(\xi,\psi) - \varepsilon\nabla\Phi_i^{(1)}(\xi,\psi) - \cdots \tag{28}$$

where the subscript i implies 1 or 2 for the air gap and for the permanent magnets, respectively. By substituting Eq. (26) and (27) into the field equations (20) and (21) and by expanding for small ε, the following groups of the equations and their boundary

conditions are derived. By collecting coefficients of like powers of ε, the zeroth-order equations become

$$\frac{\partial^2 \Phi_1^{(0)}}{\partial \xi^2}+\frac{1}{\xi}\frac{\partial \Phi_1^{(0)}}{\partial \xi}+\frac{1}{\xi^2}\frac{\partial^2 \Phi_1^{(0)}}{\partial \psi^2}=0 \tag{29}$$

$$\frac{\partial^2 \Phi_2^{(0)}}{\partial \xi^2}+\frac{1}{\xi}\frac{\partial \Phi_2^{(0)}}{\partial \xi}+\frac{1}{\xi^2}\frac{\partial^2 \Phi_2^{(0)}}{\partial \psi^2}=\frac{1}{\mu_r}\frac{M_\xi}{\xi} \tag{30}$$

The zeroth-order boundary condition at $\xi = R_s$, is

$$-\mu_0 \frac{\partial \Phi_1^{(0)}(\xi,\psi)}{\partial \xi}\Big|_{\xi=R_s}=\sum_{n=1,3,5\ldots}^{\infty}\sum_{m=0}^{\infty} X_{nm}\left\{\cos[(np+mq)\psi+mq\omega t]+\cos[(np-mq)\psi-mq\omega t]\right\} \tag{31}$$

and at $\xi = R_r$,

$$-\frac{1}{\xi}\frac{\partial \Phi_2^{(0)}(\xi,\psi)}{\partial \psi}\Big|_{\xi=R_r}=0 \tag{32}$$

which means that the permeability of the rotor back iron is infinite. At the boundary of the air gap and the permanent magnet region, the following two conditions should be satisfied

$$-\mu_0 \frac{\partial \Phi_1^{(0)}(\xi,\psi)}{\partial \xi}\Big|_{\xi=R_m}=-\mu_0\mu_r \frac{\partial \Phi_2^{(0)}(\xi,\psi)}{\partial \xi}\Big|_{\xi=R_m}+\mu_0 M_\xi\Big|_{\xi=R_m} \tag{33}$$

and

$$-\frac{1}{\xi}\frac{\partial \Phi_1^{(0)}(\xi,\psi)}{\partial \psi}\Big|_{\xi=R_m}=-\frac{1}{\xi}\frac{\partial \Phi_2^{(0)}(\xi,\psi)}{\partial \psi}\Big|_{\xi=R_m} \tag{34}$$

in which the continuity of the flux density flow in the normal direction and the field intensity in the tangential direction is commissioned.

The first-order equations are

$$\frac{\partial^2 \Phi_1^{(1)}}{\partial \xi^2} + \frac{1}{\xi}\frac{\partial \Phi_1^{(1)}}{\partial \psi} + \frac{1}{\xi^2}\frac{\partial^2 \Phi_1^{(1)}}{\partial \psi^2} = 0 \tag{35}$$

$$\frac{\partial^2 \Phi_2^{(1)}}{\partial \xi^2} + \frac{1}{\xi}\frac{\partial \Phi_2^{(1)}}{\partial \psi} + \frac{1}{\xi^2}\frac{\partial^2 \Phi_2^{(1)}}{\partial \psi^2} = 0 \tag{36}$$

Note that unlike the zeroth order equation in the permanent magnet region, there is no forcing term because the permanent magnet distribution is symmetric with respect to the moving coordinates.

The first order boundary condition at the outer surface of the stator $\xi = R_s$, is

$$\begin{aligned} -\mu_0 \frac{\partial \Phi_1^{(1)}(\xi,\psi)}{\partial \xi}\Big|_{\xi=R_s} - \mu_0 \frac{\partial^2 \Phi_1^{(0)}(\xi,\psi)}{\partial \xi^2}\Big|_{\xi=R_s} \cos(\psi + \omega t - \varphi) \\ = \sum_{n=1,3,5\ldots}^{\infty} \sum_{m=0}^{\infty} Y_{nm} \Big\{ \cos[(np+mq-1)\psi + (mq-1)\omega t + \varphi] \\ + \cos[(np-mq-1)\psi - (mq+1)\omega t + \varphi] \Big\} \\ + \sum_{n=1,3,5\ldots}^{\infty} \sum_{m=0}^{\infty} Z_{nm} \Big\{ \cos[(np+mq+1)\psi + (mq+1)\omega t - \varphi] \\ + \cos[(np-mq+1)\psi - (mq-1)\omega t - \varphi] \Big\} \end{aligned} \tag{37}$$

and at the boundary of the PM and the rotor back iron,

$$-\frac{1}{\xi}\frac{\partial \Phi_2^{(1)}(\xi,\psi)}{\partial \psi}\Big|_{\xi=R_r} = 0 \tag{38}$$

And the other conditions at the boundary of the air gap and the permanent magnet region are

$$-\mu_0 \frac{\partial \Phi_1^{(1)}(\xi,\psi)}{\partial \xi}\Big|_{\xi=R_m} = -\mu_0 \mu_r \frac{\partial \Phi_2^{(1)}(\xi,\psi)}{\partial \xi}\Big|_{\xi=R_m} \tag{39}$$

$$-\frac{1}{\xi}\frac{\partial \Phi_1^{(1)}(\xi,\psi)}{\partial \psi}\bigg|_{\xi=R_m} = -\frac{1}{\xi}\frac{\partial \Phi_2^{(1)}(\xi,\psi)}{\partial \psi}\bigg|_{\xi=R_m} \tag{40}$$

Note again that the flux density equation in the permanent magnet region in Eq. (39) contains no extra magnetization because of the symmetricity of the permanent magnet in the moving coordinate system.

Perturbation Solutions

The zeroth-order solutions for the air gap and the permanent magnet region are proposed by considering the periodicity of the field and the slotting effect on the field as the boundary conditions.

$$\begin{aligned}\Phi_1^{(0)}(\xi,\psi) = &\sum_{n=1,3,5\ldots}^{\infty}\left(A_{1n}^0\xi^{np}+B_{1n}^0\xi^{-np}\right)\cos\left[np\psi\right]\\ &+\sum_{n=1,3,5\ldots}^{\infty}\sum_{m=0}^{\infty}\left(C_{1nm}^0\xi^{np+mq}+D_{1nm}^0\xi^{-np-mq}\right)\cos\left[(np+mq)\psi+mq\omega t\right]\\ &+\sum_{n=1,3,5\ldots}^{\infty}\sum_{m=0}^{\infty}\left(E_{1nm}^0\xi^{np-mq}+F_{1nm}^0\xi^{-np+mq}\right)\cos\left[(np-mq)\psi-mq\omega t\right]\end{aligned} \tag{41}$$

$$\begin{aligned}\Phi_2^{(0)}(\xi,\psi) = &\sum_{n=1,3,5\ldots}^{\infty}\left(A_{2n}^0\xi^{np}+B_{2n}^0\xi^{-np}\right)\cos\left[np\psi\right]\\ &+\sum_{n=1,3,5\ldots}^{\infty}\sum_{m=0}^{\infty}\left(C_{2nm}^0\xi^{np+mq}+D_{2nm}^0\xi^{-np-mq}\right)\cos\left[(np+mq)\psi+mq\omega t\right]\\ &+\sum_{n=1,3,5\ldots}^{\infty}\sum_{m=0}^{\infty}\left(E_{2nm}^0\xi^{np-mq}+F_{2nm}^0\xi^{-np+mq}\right)\cos\left[((np-mq)\psi-mq\omega t\right]\\ &+\frac{1}{\mu_r}\sum_{n=1,3,5\ldots}^{\infty}\frac{\xi\cdot M_n}{1-(np)^2}\cos\left[np\psi\right]\end{aligned} \tag{42}$$

The arbitrary constants are again obtained by substituting the boundary conditions and are the same as obtained in the case of no eccentricity as given in Appendix I. However, note

that the above solutions are expressed by the moving coordinates and the frequency contents are based on them. They can easily be transformed to the original unperturbed equations by the coordinate transform equations together with by neglecting simply the perturbative phase terms.

The first-order solutions are obtained in the followings

$$\begin{aligned}
\Phi_1^{(1)}(\xi,\psi) = & \sum_{n=1,3,5\cdots}^{\infty} \left(A_{1n}^1 \xi^{np+1} + B_{1n}^1 \xi^{-np-1}\right) \cos\left[(np+1)\psi + \omega t - \varphi\right] \\
& + \sum_{n=1,3,5\cdots}^{\infty} \left(C_{1n}^1 \xi^{np-1} + D_{1n}^1 \xi^{-np+1}\right) \cos\left[(np-1)\psi - \omega t + \varphi\right] \\
& + \sum_{n=1,3,5\cdots}^{\infty} \sum_{m=0}^{\infty} \left(E_{1nm}^1 \xi^{np+mq-1} + F_{1nm}^1 \xi^{-np-mq+1}\right) \cos\left[(np+mq-1)\psi + (mq-1)\omega t + \varphi\right] \\
& + \sum_{n=1,3,5\cdots}^{\infty} \sum_{m=0}^{\infty} \left(G_{1nm}^1 \xi^{np-mq-1} + H_{1nm}^1 \xi^{-np+mq+1}\right) \cos\left[(np-mq-1)\psi - (mq+1)\omega t + \varphi\right] \\
& + \sum_{n=1,3,5\cdots}^{\infty} \sum_{m=0}^{\infty} \left(I_{1nm}^1 \xi^{np+mq+1} + J_{1nm}^1 \xi^{-np-mq-1}\right) \cos\left[(np+mq+1)\psi + (mq+1)\omega t - \varphi\right] \\
& + \sum_{n=1,3,5\cdots}^{\infty} \sum_{m=0}^{\infty} \left(K_{1nm}^1 \xi^{np-mq+1} + L_{1nm}^1 \xi^{-np+mq-1}\right) \cos\left[(np-mq+1)\psi - (mq-1)\omega t - \varphi\right]
\end{aligned} \tag{43}$$

for the air gap region. The solution for the permanent magnet region is

$$\begin{aligned}
\Phi_2^{(1)}(\xi,\psi) = & \sum_{n=1,3,5\cdots}^{\infty} \left(A_{2n}^1 \xi^{np+1} + B_{2n}^1 \xi^{-np-1}\right) \cos\left[(np+1)\psi + \omega t - \varphi\right] \\
& + \sum_{n=1,3,5}^{\infty} \left(C_{2n}^1 \xi^{np-1} + D_{2n}^1 \xi^{-np+1}\right) \cos\left[(np-1)\psi - \omega t + \varphi\right] \\
& + \sum_{n=1,3,5\cdots}^{\infty} \sum_{m=0}^{\infty} \left(E_{2nm}^1 \xi^{np+mq-1} + F_{2nm}^1 \xi^{-np-mq+1}\right) \cos\left[(np+mq-1)\psi + (mq-1)\omega t + \varphi\right] \\
& + \sum_{n=1,3,5\cdots}^{\infty} \sum_{m=0}^{\infty} \left(G_{2nm}^1 \xi^{np-mq-1} + H_{2nm}^1 \xi^{-np+mq+1}\right) \cos\left[(np-mq-1)\psi - (mq+1)\omega t + \varphi\right]
\end{aligned}$$

$$+\sum_{n=1,3,5\cdots}^{\infty}\sum_{m=0}^{\infty}\left(I_{2nm}^{1}\xi^{np+mq+1}+J_{2nm}^{1}\xi^{-np-mq-1}\right)\cos\left[(np+mq+1)\psi(+mq+1)\omega t-\varphi\right]$$

$$+\sum_{n=1,3,5\cdots}^{\infty}\sum_{m=0}^{\infty}\left(K_{2nm}^{1}\xi^{np-mq+1}+L_{2nm}^{1}\xi^{-np+mq-1}\right)\cos\left[(np-mq+1)\psi-(mq-1)\omega t-\varphi\right]$$

(44)

Note in the above equations that the slotting effect on the field is instituted. Again the arbitrary constants can be obtained by the boundary conditions.

Flux Density Distribution in the Moving Coordinate System

The total flux density distributions in the air gap region contain the original and the additional distributions due to the rotor eccentricity. By considering the magnetic potential expressions in Eq. (26) and (27), the total flux density may be obtained by

$$B_{\xi,1}(\xi,\psi,\varepsilon)=B_{\xi,1}^{(0)}(\xi,\psi)+\varepsilon B_{\xi,1}^{(1)}(\xi,\psi)+\cdots \tag{45}$$

$$B_{\psi,1}(\xi,\psi,\varepsilon)=B_{\psi,1}^{(0)}(\xi,\psi)+\varepsilon B_{\psi,1}^{(1)}(\xi,\psi)+\cdots \tag{46}$$

where the original flux density distributions are obtained from

$$B_{\xi,1}^{(0)}(\xi,\psi)=-\mu_0\frac{\partial\Phi_1^{(0)}(\xi,\psi)}{\partial\xi} \tag{47}$$

$$B_{\psi,1}^{(0)}(\xi,\psi)=-\frac{\mu_0}{\xi}\frac{\partial\Phi_1^{(0)}(\xi,\psi)}{\partial\psi} \tag{48}$$

and the additional flux density due to the rotor eccentricity is determined by

$$B_{\xi,1}^{(1)}(\xi,\psi)=-\mu_0\frac{\partial\Phi_1^{(1)}(\xi,\psi)}{\partial\xi} \tag{49}$$

$$B_{\psi,1}^{(1)}(\xi,\psi)=-\frac{\mu_0}{\xi}\frac{\partial\Phi_1^{(1)}(\xi,\psi)}{\partial\psi} \tag{50}$$

Then, from the magnetic potential distributions in the air gap in Eq. (41-44), the flux density distributions are given by

$$
\begin{aligned}
B_{\xi,1}(\xi,\psi,\varepsilon) = &-\mu_0 \sum_{n=1,3,5\cdots}^{\infty} (np)\hat{A}_{1n}^{0}\left(\bar{\xi}^{\,np-1} - \bar{r}_s^{\,2np}\bar{\xi}^{\,-np-1}\right)\cos\left[np\psi\right] \\
&-\mu_0 \sum_{n=1,3,5\cdots}^{\infty}\sum_{m=0}^{\infty}\left(\hat{C}_{1nm}^{0}\bar{\xi}^{\,np+mq-1} - \hat{D}_{1nm}^{0}\bar{\xi}^{\,-np-mq-1}\right)\cos\left[\left(np+mq\right)\psi + mq\omega t\right] \\
&-\mu_0 \sum_{n=1,3,5\cdots}^{\infty}\sum_{m=0}^{\infty}\left(\hat{E}_{1nm}^{0}\bar{\xi}^{\,np-mq-1} - \hat{F}_{1nm}^{0}\bar{\xi}^{\,-np+mq-1}\right)\cos\left[\left(np-mq\right)\psi - mq\omega t\right] \\
&-\varepsilon\mu_0 \sum_{n=1,3,5\cdots}^{\infty}\frac{1}{\xi}\left(\hat{A}_{1n}^{1}\bar{\xi}^{\,np+1} - \hat{B}_{1n}^{1}\bar{\xi}^{\,-np-1}\right)\cos\left[\left(np+1\right)\psi + \omega t - \varphi\right] \\
&-\varepsilon\mu_0 \sum_{n=1,3,5\cdots}^{\infty}\frac{1}{\xi}\left(\hat{C}_{1n}^{1}\bar{\xi}^{\,np-1} - \hat{D}_{1n}^{1}\bar{\xi}^{\,-np+1}\right)\cos\left[\left(np-1\right)\psi - \omega t + \varphi\right] \\
&-\varepsilon\mu_0 \sum_{n=1,3,5\cdots}^{\infty}\sum_{m=0}^{\infty}\frac{1}{\xi}\left(\hat{E}_{1nm}^{1}\bar{\xi}^{\,np+mq-1} - \hat{F}_{1nm}^{1}\bar{\xi}^{\,-np-mq+1}\right)\cos\left[\left(np+mq-1\right)\psi + \left(mq-1\right)\omega t + \varphi\right] \\
&-\varepsilon\mu_0 \sum_{n=1,3,5\cdots}^{\infty}\sum_{m=0}^{\infty}\frac{1}{\xi}\left(\hat{G}_{1nm}^{1}\bar{\xi}^{\,np-mq-1} - \hat{H}_{1nm}^{1}\bar{\xi}^{\,-np+mq+1}\right)\cos\left[\left(np-mq-1\right)\psi - \left(mq+1\right)\omega t + \varphi\right] \\
&-\varepsilon\mu_0 \sum_{n=1,3,5\cdots}^{\infty}\sum_{m=0}^{\infty}\frac{1}{\xi}\left(\hat{I}_{1nm}^{1}\bar{\xi}^{\,np+mq+1} - \hat{J}_{1nm}^{1}\bar{\xi}^{\,-np-mq-1}\right)\cos\left[\left(np+mq+1\right)\psi + \left(mq+1\right)\omega t - \varphi\right] \\
&-\varepsilon\mu_0 \sum_{n=1,3,5\cdots}^{\infty}\sum_{m=0}^{\infty}\frac{1}{\xi}\left(\hat{K}_{1nm}^{1}\bar{\xi}^{\,np-mq+1} - \hat{L}_{1nm}^{1}\bar{\xi}^{\,-np+mq-1}\right)\cos\left[\left(np-mq+1\right)\psi - \left(mq-1\right)\omega t - \varphi\right]
\end{aligned}
\tag{51}
$$

$$
\begin{aligned}
B_{\psi,1}(\xi,\psi,\varepsilon) = &\mu_0 \sum_{n=1,3,5\cdots}^{\infty} (np)\hat{A}_{1n}^{0}\left(\bar{\xi}^{\,np-1} + \bar{r}_s^{\,2np}\bar{\xi}^{\,-np-1}\right)\sin\left[np\psi\right] \\
&+\mu_0 \sum_{n=1,3,5\cdots}^{\infty}\sum_{m=0}^{\infty}\left(\hat{C}_{1nm}^{0}\bar{\xi}^{\,np+mq-1} + \hat{D}_{1nm}^{0}\bar{\xi}^{\,-np-mq-1}\right)\sin\left[\left(np+mq\right)\psi + mq\omega t\right] \\
&+\mu_0 \sum_{n=1,3,5\cdots}^{\infty}\sum_{m=0}^{\infty}\left(\hat{E}_{1nm}^{0}\bar{\xi}^{\,np-mq-1} + \hat{F}_{1nm}^{0}\bar{\xi}^{\,-np+mq-1}\right)\sin\left[\left(np-mq\right)\psi - mq\omega t\right]
\end{aligned}
$$

$$+\varepsilon\mu_0 \sum_{n=1,3,5\cdots}^{\infty} \frac{1}{\xi}\left(\hat{A}_{1n}^{1}\bar{\xi}^{\,np+1}+\hat{B}_{1n}^{1}\bar{\xi}^{\,-np-1}\right)\sin\left[(np+1)\psi+\omega t-\varphi\right]$$

$$+\varepsilon\mu_0 \sum_{n=1,3,5\cdots}^{\infty} \frac{1}{\xi}\left(\hat{C}_{1n}^{1}\bar{\xi}^{\,np-1}+\hat{D}_{1n}^{1}\bar{\xi}^{\,-np+1}\right)\sin\left[(np-1)\psi-\omega t+\varphi\right]$$

$$+\varepsilon\mu_0 \sum_{n=1,3,5\cdots}^{\infty}\sum_{m=0}^{\infty} \frac{1}{\xi}\left(\hat{E}_{1nm}^{1}\bar{\xi}^{\,np+mq-1}+\hat{F}_{1nm}^{1}\bar{\xi}^{\,-np-mq+1}\right)\sin\left[(np+mq-1)\psi+(mq-1)\omega t+\varphi\right]$$

$$+\varepsilon\mu_0 \sum_{n=1,3,5\cdots}^{\infty}\sum_{m=0}^{\infty} \frac{1}{\xi}\left(\hat{G}_{1nm}^{1}\bar{\xi}^{\,np-mq-1}+\hat{H}_{1nm}^{1}\bar{\xi}^{\,-np+mq+1}\right)\sin\left[(np-mq-1)\psi-(mq+1)\omega t+\varphi\right]$$

$$+\varepsilon\mu_0 \sum_{n=1,3,5\cdots}^{\infty}\sum_{m=0}^{\infty} \frac{1}{\xi}\left(\hat{I}_{1nm}^{1}\bar{\xi}^{\,np+mq+1}+\hat{J}_{1nm}^{1}\bar{\xi}^{\,-np-mq-1}\right)\sin\left[(np+mq+1)\psi+(mq+1)\omega t-\varphi\right]$$

$$+\varepsilon\mu_0 \sum_{n=1,3,5\cdots}^{\infty}\sum_{m=0}^{\infty} \frac{1}{\xi}\left(\hat{K}_{1nm}^{1}\bar{\xi}^{\,np-mq+1}+\hat{L}_{1nm}^{1}\bar{\xi}^{\,-np+mq-1}\right)\sin\left[(np-mq+1)\psi-(mq-1)\omega t-\varphi\right]$$

(52)

where the arbitrary constants are again given in a normalized form for easy numerical evaluation in Appendix II and $\bar{\xi}=\frac{\xi}{R_r}$ also represents a normalized position.

Flux Density Distribution in the Fixed Coordinate System

Flux density distributions which are expressed in terms of the moving coordinates are not suitable for other further calculations such as unbalanced magnetic force and cogging torque. Therefore, they need to be transformed into the ones in the fixed coordinate system. The detailed transforming procedure is explained in [3].

By using the same procedure, the air gap flux density components are represented in a perturbation form

$$\overline{B}_{r,1}(r,\theta,\varepsilon)=-\mu_0\frac{\partial \Phi_1^{(0)}(\xi,\psi)}{\partial \xi}-\varepsilon\mu_0\left\{\frac{\partial \Phi_1^{(1)}(\xi,\psi)}{\partial \xi}-\frac{1}{r^2}\frac{\partial \Phi_1^{(0)}(\xi,\psi)}{\partial \psi}\sin(\theta-\phi)\right\} \tag{53}$$

$$\overline{B}_{\theta,1}(r,\theta,\varepsilon)=-\frac{\mu_0}{r}\frac{\partial \Phi_1^{(0)}(\xi,\psi)}{\partial \psi}$$

$$-\varepsilon\mu_0\left\{\frac{1}{r}\frac{\partial \Phi_1^{(1)}(\xi,\psi)}{\partial \psi}+\frac{1}{r}\frac{\partial \Phi_1^{(0)}(\xi,\psi)}{\partial \xi}\sin(\theta-\phi)+\frac{1}{r^2}\frac{\partial \Phi_1^{(0)}(\xi,\psi)}{\partial \psi}\cos(\theta-\phi)\right\} \tag{54}$$

By substituting the coordinate transformation equations (13) and (14) into the above expressions and linearizing them around the radius of the stator outer surface R_s, the required flux density distributions are obtained in terms of the fixed coordinates

$$\overline{B}_{r,1}(r,\theta,\varepsilon)=-\mu_0\sum_{n=1,3,5\cdots}^{\infty}(np)\hat{A}_{1n}^{0}\left(\bar{r}^{np-1}-\bar{r}_s^{2np}\bar{r}^{-np-1}\right)\cos\left[np(\theta-\omega t)\right]$$

$$-\mu_0\sum_{n=1,3,5\cdots}^{\infty}\sum_{m=0}^{\infty}\left(\hat{C}_{1nm}^{0}\bar{r}^{np+mq-1}-\hat{D}_{1nm}^{0}\bar{r}^{-np-mq-1}\right)\cos\left[(np+mq)\theta-np\omega t\right]$$

$$-\mu_0\sum_{n=1,3,5\cdots}^{\infty}\sum_{m=0}^{\infty}\left(\hat{E}_{1nm}^{0}\bar{r}^{np-mq-1}-\hat{F}_{1nm}^{0}\bar{r}^{-np+mq-1}\right)\cos\left[(np-mq)\theta-np\omega t\right]$$

$$-\varepsilon\frac{\mu_0}{2r}\sum_{n=1,3,5\cdots}^{\infty}\sum_{m=0}^{\infty}\left[np\hat{A}_{1n}^{0}\left\{np\bar{r}^{np-1}+(np+2)\bar{r}_s^{2np}\bar{r}^{-np-1}\right\}+2\left(\hat{A}_{1n}^{1}\bar{r}^{np+1}-\hat{B}_{1n}^{1}\bar{r}^{-np-1}\right)\right]$$

$$\cdot\cos\left[(np+1)\theta-np\omega t-\varphi\right]$$

$$-\varepsilon\frac{\mu_0}{2r}\sum_{n=1,3,5\cdots}^{\infty}\sum_{m=0}^{\infty}\left[np\hat{A}_{1n}^{0}\left\{(np-2)\bar{r}^{np-1}+np\bar{r}_s^{2np}\bar{r}^{-np-1}\right\}+2\left(\hat{C}_{1n}^{1}\bar{r}^{np-1}-\hat{D}_{1n}^{1}\bar{r}^{-np+1}\right)\right]$$

$$\cdot\cos\left[(np-1)\theta-np\omega t+\varphi\right]$$

$$-\varepsilon\frac{\mu_0}{2r}\sum_{n=1,3,5\cdots}^{\infty}\sum_{m=0}^{\infty}\left[\left\{(np+mq-2)\hat{C}_{1n}^{0}\bar{r}^{np+mq-1}+(np+mq)\hat{D}_{1n}^{0}\bar{r}^{-np-mq-1}\right\}\right.$$

$$\left.+2\left(\hat{E}_{1nm}^{1}\bar{r}^{np+mq-1}-\hat{F}_{1nm}^{1}\bar{r}^{-np-mq+1}\right)\right]\cos\left[(np+mq-1)\theta-np\omega t+\varphi\right]$$

$$-\varepsilon\frac{\mu_0}{2r}\sum_{n=1,3,5\cdots}^{\infty}\sum_{m=0}^{\infty}\Big[\big\{(np-mq-2)\hat{E}_{1n}^{0}\bar{r}^{np-mq-1}+(np-mq)\hat{F}_{1n}^{0}\bar{r}^{-np+mq-1}\big\}$$

$$+2\big(\hat{G}_{1nm}^{1}\bar{r}^{np+mq-1}-\hat{H}_{1nm}^{1}\bar{r}^{-np-mq+1}\big)\Big]\cos\Big[(np-mq-1)\theta-np\omega t+\varphi\Big]$$

$$-\varepsilon\frac{\mu_0}{2r}\sum_{n=1,3,5\cdots}^{\infty}\sum_{m=0}^{\infty}\Big[\big\{(np+mq)\hat{C}_{1n}^{0}\bar{r}^{np+mq-1}-(np+mq+2)\hat{D}_{1n}^{0}\bar{r}^{-np-mq-1}\big\}$$

$$+2\big(\hat{I}_{1nm}^{1}\bar{r}^{np+mq+1}-\hat{J}_{1nm}^{1}\bar{r}^{-np-mq-1}\big)\Big]\cos\Big[(np+mq+1)\theta-np\omega t-\varphi\Big]$$

$$-\varepsilon\frac{\mu_0}{2r}\sum_{n=1,3,5\cdots}^{\infty}\sum_{m=0}^{\infty}\Big[\big\{(np-mq)\hat{E}_{1n}^{0}\bar{r}^{np-mq-1}-(np-mq+2)\hat{F}_{1n}^{0}\bar{r}^{-np+mq-1}\big\}$$

$$+2\big(\hat{K}_{1nm}^{1}\bar{r}^{np+mq-1}-\hat{L}_{1nm}^{1}\bar{r}^{-np-mq+1}\big)\Big]\cos\Big[(np-mq+1)\theta-np\omega t-\varphi\Big]$$

(55)

$$\bar{B}_{\theta,1}(r,\theta,\varepsilon)=\mu_0\sum_{n=1,3,5\cdots}^{\infty}(np)\hat{A}_{1n}^{0}\big(\bar{r}^{np-1}+\bar{r}_s^{2np}\bar{r}^{-np-1}\big)\sin\big[np(\theta-\omega t)\big]$$

$$+\mu_0\sum_{n=1,3,5\cdots}^{\infty}\sum_{m=0}^{\infty}\big(\hat{C}_{1nm}^{0}\bar{r}^{np+mq-1}+\hat{D}_{1nm}^{0}\bar{r}^{-np-mq-1}\big)\sin\big[(np+mq)\theta-np\omega t\big]$$

$$+\mu_0\sum_{n=1,3,5\cdots}^{\infty}\sum_{m=0}^{\infty}\big(\hat{E}_{1nm}^{0}\bar{r}^{np-mq-1}+\hat{F}_{1nm}^{0}\bar{r}^{-np+mq-1}\big)\sin\big[(np-mq)\theta-np\omega t\big]$$

$$+\varepsilon\frac{\mu_0}{2r}\sum_{n=1,3,5\cdots}^{\infty}\sum_{m=0}^{\infty}\Big[np\hat{A}_{1n}^{0}\big\{np\bar{r}^{np-1}-(np+2)\bar{r}_s^{2np}\bar{r}^{-np-1}\big\}-2\big(\hat{A}_{1n}^{1}\bar{r}^{np+1}+\hat{B}_{1n}^{1}\bar{r}^{-np-1}\big)\Big]$$

$$\cdot\sin\Big[(np+1)\theta-np\omega t-\varphi\Big]$$

$$+\varepsilon\frac{\mu_0}{2r}\sum_{n=1,3,5\cdots}^{\infty}\sum_{m=0}^{\infty}\Big[np\hat{A}_{1n}^{0}\big\{(np-2)\bar{r}^{np-1}-np\bar{r}_s^{2np}\bar{r}^{-np-1}\big\}-2\big(\hat{C}_{1n}^{1}\bar{r}^{np-1}+\hat{D}_{1n}^{1}\bar{r}^{-np+1}\big)\Big]$$

$$\cdot\sin\Big[(np-1)\theta-np\omega t+\varphi\Big]$$

$$+\varepsilon\frac{\mu_0}{2r}\sum_{n=1,3,5\cdots}^{\infty}\sum_{m=0}^{\infty}\Big[\big\{(np+mq-2)\hat{C}_{1n}^{0}\bar{r}^{np+mq-1}-(np+mq)\hat{D}_{1n}^{0}\bar{r}^{-np-mq-1}\big\}$$

$$-2\big(\hat{E}_{1nm}^{1}\bar{r}^{np+mq-1}+\hat{F}_{1nm}^{1}\bar{r}^{-np-mq+1}\big)\Big]\sin\Big[(np+mq-1)\theta-np\omega t+\varphi\Big]$$

$$+\varepsilon\frac{\mu_0}{2r}\sum_{n=1,3,5\cdots}^{\infty}\sum_{m=0}^{\infty}\Big[\Big\{(np+mq)\hat{C}_{1n}^{0}\bar{r}^{np+mq-1}-(np+mq+2)\hat{D}_{1n}^{0}\bar{r}^{-np-mq-1}\Big\}$$

$$-2\Big(\hat{I}_{1nm}^{1}\bar{r}^{np+mq+1}+\hat{J}_{1nm}^{1}\bar{r}^{-np-mq-1}\Big)\Big]\sin\Big[(np+mq+1)\theta-np\omega t-\varphi\Big]$$

$$+\varepsilon\frac{\mu_0}{2r}\sum_{n=1,3,5\cdots}^{\infty}\sum_{m=0}^{\infty}\Big[\Big\{(np+mq-2)\hat{E}_{1n}^{0}\bar{r}^{np-mq-1}-(np-mq)\hat{F}_{1n}^{0}\bar{r}^{-np+mq-1}\Big\}$$

$$-2\Big(\hat{G}_{1nm}^{1}\bar{r}^{np-mq-1}+\hat{H}_{1nm}^{1}\bar{r}^{-np+mq+1}\Big)\Big]\sin\Big[(np-mq-1)\theta-np\omega t+\varphi\Big]$$

$$+\varepsilon\frac{\mu_0}{2r}\sum_{n=1,3,5\cdots}^{\infty}\sum_{m=0}^{\infty}\Big[\Big\{(np-mq)\hat{E}_{1n}^{0}\bar{r}^{np-mq-1}-(np-mq+2)\hat{F}_{1n}^{0}\bar{r}^{-np+mq-1}\Big\}$$

$$-2\Big(\hat{K}_{1nm}^{1}\bar{r}^{np-mq+1}+\hat{L}_{1nm}^{1}\bar{r}^{-np+mq-1}\Big)\Big]\sin\Big[(np-mq+1)\theta-np\omega t-\varphi\Big] \tag{56}$$

where $\bar{r}=\dfrac{r}{R_r}$

COMPARISON OF THE ANALYTIC AND FINITE ELEMENT CALCULATION

The objective of this section is to verify the accuracy of the analytical method explained in the present paper. This is accomplished by comparing the radial and circumferential flux density distributions in the air gap with those obtained from a corresponding finite element analysis, which is widely considered as very accurate. The design parameters of prototype motors with an external rotor motor used in hard disk drives are listed in Appendix III.

The finite element analysis was executed on a magnetic finite element analysis package, TOSCA with a pre- and post-processor called OPERA. There are several difficulties involved in generating a finite element mesh for the motor. Firstly, the first example of an 8 pole/9slot motor is not symmetric itself and the second example of a 12

pole/9 slot motor is not symmetric when it has the rotor eccentricity, so the entire motor must be modeled. Secondly, a uniform discretization of the mesh in the entire motor was desired to minimize the amount of the modeling due to the size limitations of the finite element solver. Therefore, tooth slots and permanent magnet slots are modeled on the radial line with specified angle spans. The final mesh has 576 elements circumferentially along the air gap. With quadratic elements defined along the air gap, the mesh has approximately 108,864 nodes. The finite element analysis was executed with the linear magnetic material properties of the back iron and the rotor magnets. The relative permeability of the stator and the rotor back iron, μ_r is 1364 though it was assumed to be infinite in the perturbation analysis. Because of the finite permeability of the back iron, the boundary conditions of the finite element analysis were given as far field conditions with which the scalar potential was assumed to be zero along the boundary lines at a distance from the back irons.

The finite element model was built on the moving coordinate system because of a relative simplicity of expressing the rotor magnet directions. The results are, therefore, compared with those calculated by Eq. (51) and (52).

Fig. 4 shows the flux density distributions of the air gap in the radial and circumferential direction. The flux density distributions were calculated at the outer surface of the stator of motor I. The relative permeance function by Zhu [5] was utilized for the calculation. The radial flux density obtained by the analytical method clearly follows the one calculated by the finite element method, both in amplitude and waveform, except for at the angular positions where the edges of a stator tooth are located. The finite element calculation predicts an increase in the flux density at the tooth tips, because of

their flux concentrating effect, whereas the analytical solution dose not. This error may result from the inability of the relative permeance function to express the flux concentrating effect. The circumferential flux density distribution obtained by the analytical method shows a small discrepancy from the finite element calculation. But it is believed that the finite element solution itself may include some errors from the uniform and relatively coarse mesh generation around the slots.

Fig. 5 shows the flux density distributions obtained in the middle of the air gap at a distance of $R_s+0.5g$ from the center of the stator. The results from the analytical method and the finite element method are in good agreement. The slotting effect on the flux density inside the air gap is clearly detected in Fig. 5. Unlike in Fig. 4, the circumferential flux density calculated inside of the air gap shows good agreement both in amplitude and waveform. Therefore, it may be more advantageous to use the flux density inside the air gap for the calculation of magnetic forces such as unbalanced magnet force and cogging torque rather than the one obtained at the outer surface of the stator.

Fig. 6 shows the effect of the rotor eccentricity on the flux density in the air gap. The flux density was calculated along a circular loop inside the air gap at a distance of $R_s+0.2g$ from the center of the stator when $\varepsilon=0.5g$, which is relatively large in a permanent magnet motor. However, the flux density which was analytically calculated by the perturbation method is in good agreement with the density calculated by the finite element method despite the large eccentricity. Fig. 6 justifies the conjecture previously made in Eq. (16) that the relative permeance function of the eccentric air gap field may be represented by the one calculated from the model of the original air gap field with little error.

Fig. 7 illustrates a comparison of the flux density distributions obtained by both methods at an instance of $\omega t = 14.5^o$ and $\varphi = 45^o$. Motor II was used for the calculation with the rotor eccentricity of $\varepsilon = 0.1g$. The figures show the effects of the dead angle of the permanent magnets on the flux density distributions in both directions. With a relatively large slot opening angle of 8 degree, the analytical solution slightly underestimates the finite element result in the radial direction. The discrepancy may decrease if there exists a better expression of the relative permeance function for a relatively large slot opening. Note that the slot opening angle is considered only in expressing the relative permeance function. Aside from that, the analytical method explained in the present paper can make a very good prediction on the magnetic field with the linear characteristics of the material assumed. The average error between the analytical and the finite element results was examined to be less than about two percent.

CONCLUSION

An accurate analytical method has been developed to predict the magnetic field distribution in the air gap region of a permanent magnet motor. The method has been refined to account for the effect of slotting and the rotor eccentricity on the field distribution. The analytical method has been verified by the corresponding finite element model. The effect of slotting is included by a redefined boundary condition at the outer surface of the stator by an aid of a relative permeance function for a simplified slot model. A perturbation technique was introduced to model the rotor eccentricity which may be an inherent working mode in a spindle motor supported by fluid film bearings. The analytical results show that the magnetic field can be represented by a linear

combination of the original field with a smooth stator surface and the additional field caused by the slotting effect of the boundary. The comparison between the analytical and the finite element solutions shows that the analytical method can predict more correctly the field distribution inside the air gap region rather than in the region adjacent to the stator surface. This fact may result from either an incomplete expression of the relative permeance function on the flux concentrating effect around the teeth, or the uniformity and coarseness of the finite elements in the air gap. The rotor eccentricity can be included in the analytical method by a perturbation technique. The perturbation method is very capable of effectively calculating the eccentric magnetic field despite some assumptions made for simplicity of solving procedure. The analytical method can be utilized to provide a fast design and analysis tool for evaluating the magnetic forces, which is otherwise a very time consuming if a conventional finite element method is used.

ACKNOWLEDGMENTS

The authors gratefully acknowledge The Computer Mechanics Laboratory in The University of California at Berkeley for its support of this work.

REFERENCES

[1] M. Jufer, “Brushless DC motors - Gap permeance and PM-MMF distribution analysis,” *16th Annu. Sym. Incremental Motion Control Systems and Devices*, May 1987, pp. 21-25.

[2] Z. Q. Zhu and D. Howe, “Instantaneous magnetic field distribution in brushless permanent magnet Dc motors; Part III: Effect of stator slotting,” *IEEE Trans. on Magnetics*, Vol. 29, No. 1, Jan. 1993, pp. 143-151.

[3] U. Kim and D. K. Lieu, “Magnetic field calculation in permanent magnet motors with rotor eccentricity,” *(in publication)*

[4] Z. J. Liu, C. Bi, Q. D. Zhang, M. A. Jabbar, and T. S. Low, “Electro-magnetic design for hard disk drive spindle motors with fluid film lubrication bearings,” *IEEE trans. on Magnetics*, Vol. 32 No. 5, Sept. 1996, pp. 3893-3895.

[5] Z. Q. Zhu, D. Howe, E. Bolte, and B. Ackermann “Instantaneous magnetic field distribution in brushless permanent magnet DC motors, Part I: Open-circuit field,” *IEEE Trans. on Magnetics*, Vol. 29, No. 1, Jan. 1993, pp. 124-135.

[6] K. J. Binns, P. J. Lawrenson, and C. W. Trowbridge, *The analytical and numerical solution of electric and magnetic fields*, John and Wiley and sons, 1992.

[7] G. F. Carrier and C. E. Pearson, *Partial differential equations : Theory and technique*, Academic Press, 1976.

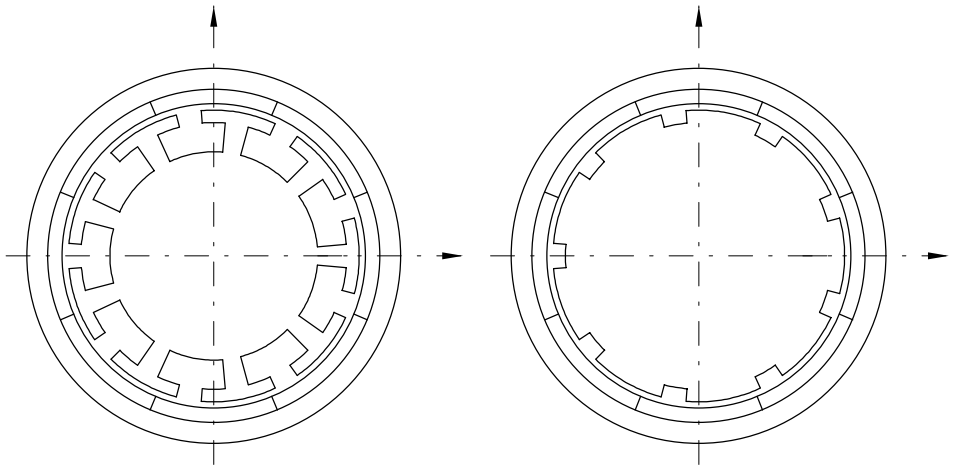

Fig. 1. Model of an 8 pole/9 slot brushless permanent magnet motor.

(a) Finite element model. (b) Analytical calculation model.

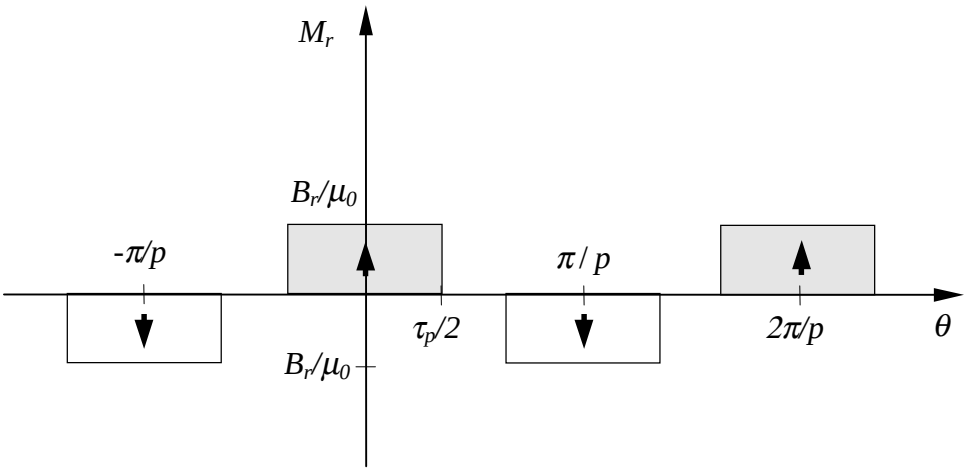

$$M_r = \sum_{n=1,3,5\cdots}^{\infty} 2\alpha_p \left(B_r/\mu_0\right) \frac{\sin\left(n\pi\alpha_p/2\right)}{\left(n\pi\alpha_p/2\right)} \cos\left(np\theta\right)$$

and $M_\theta = 0$

where the magnet pole-arc to pole-pitch ratio, $\alpha_p = \tau_p/\left(\pi/p\right)$

Fig. 2. Radial magnetization and its Fourier series expression.

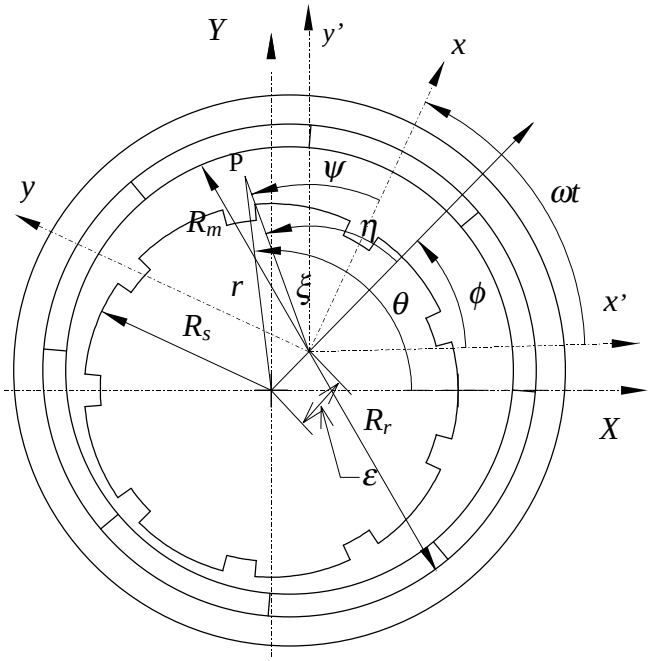

Fig. 3. Schematic diagram of a motor with the rotor eccentricity and its geometric parameters.

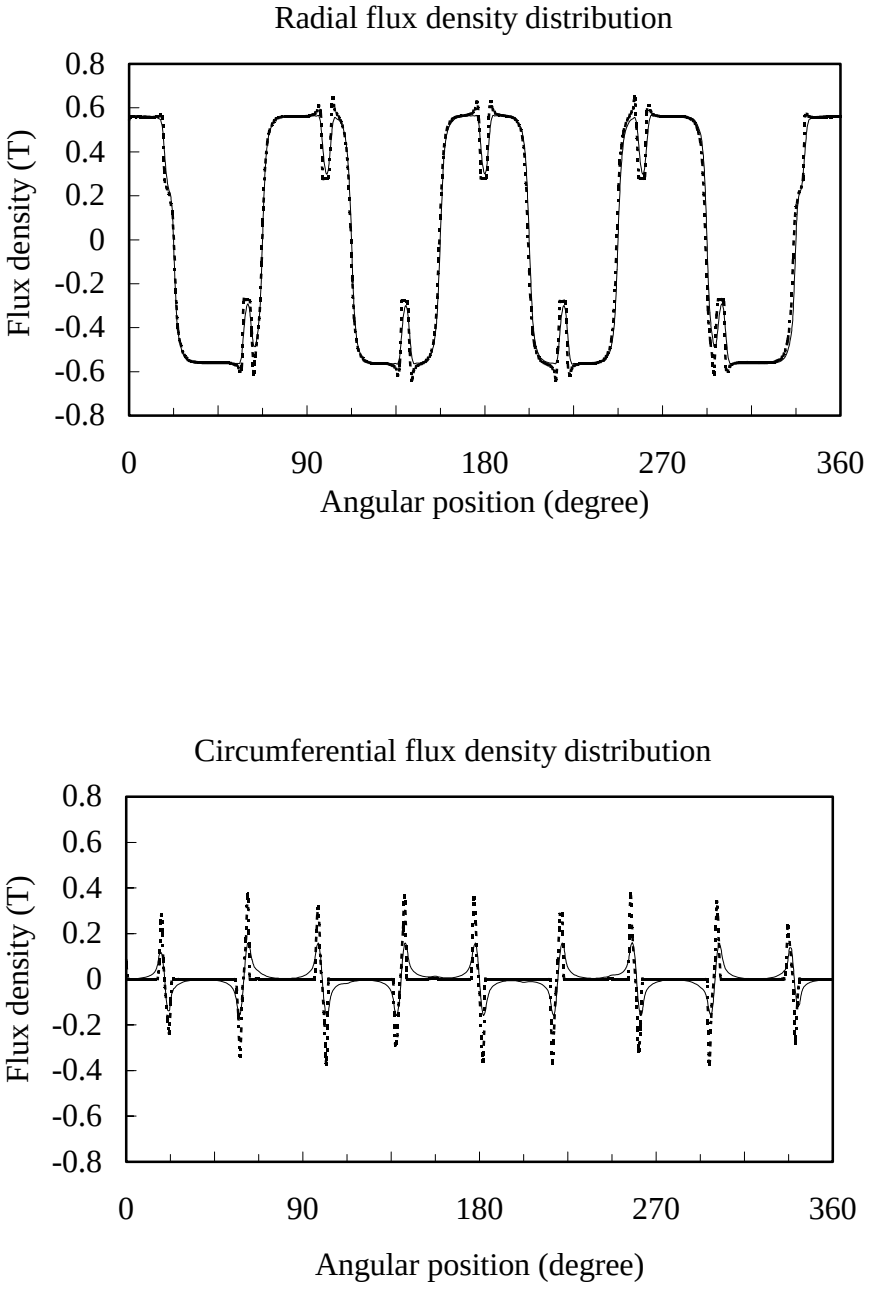

Fig. 4. Flux density distributions at the stator outer surface of motor I.

Solid line : analytical results; dotted line : FEM results.

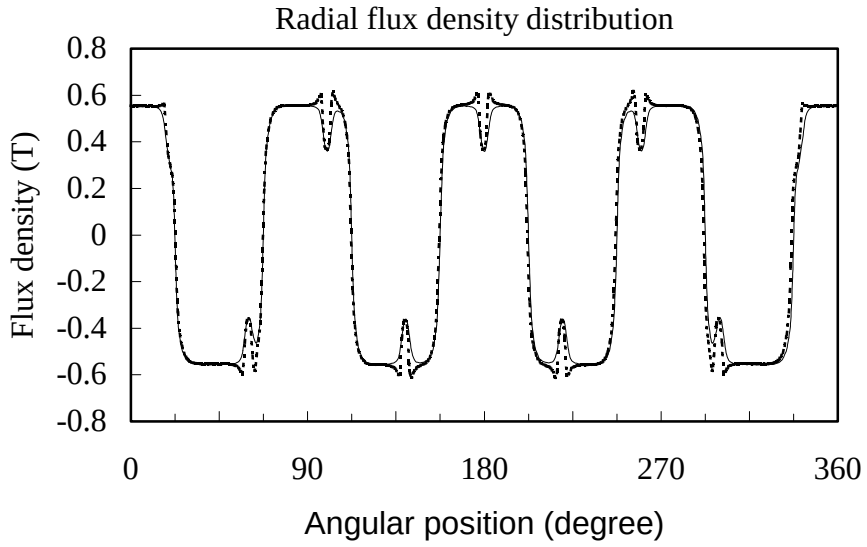

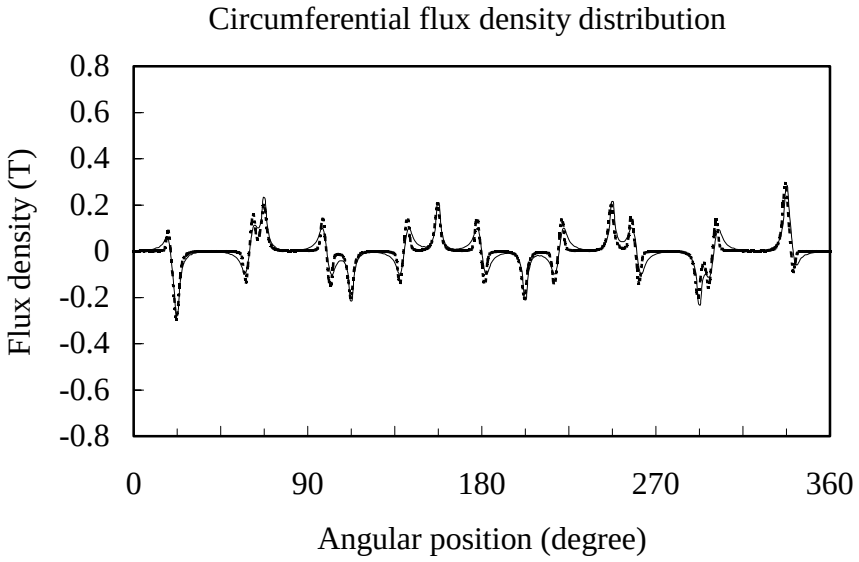

Fig. 5. Flux density distributions in the middle of the air gap *(R_s+0.5g)* between the rotor and the stator of motor I. Solid line : analytical results; dotted line : FEM results

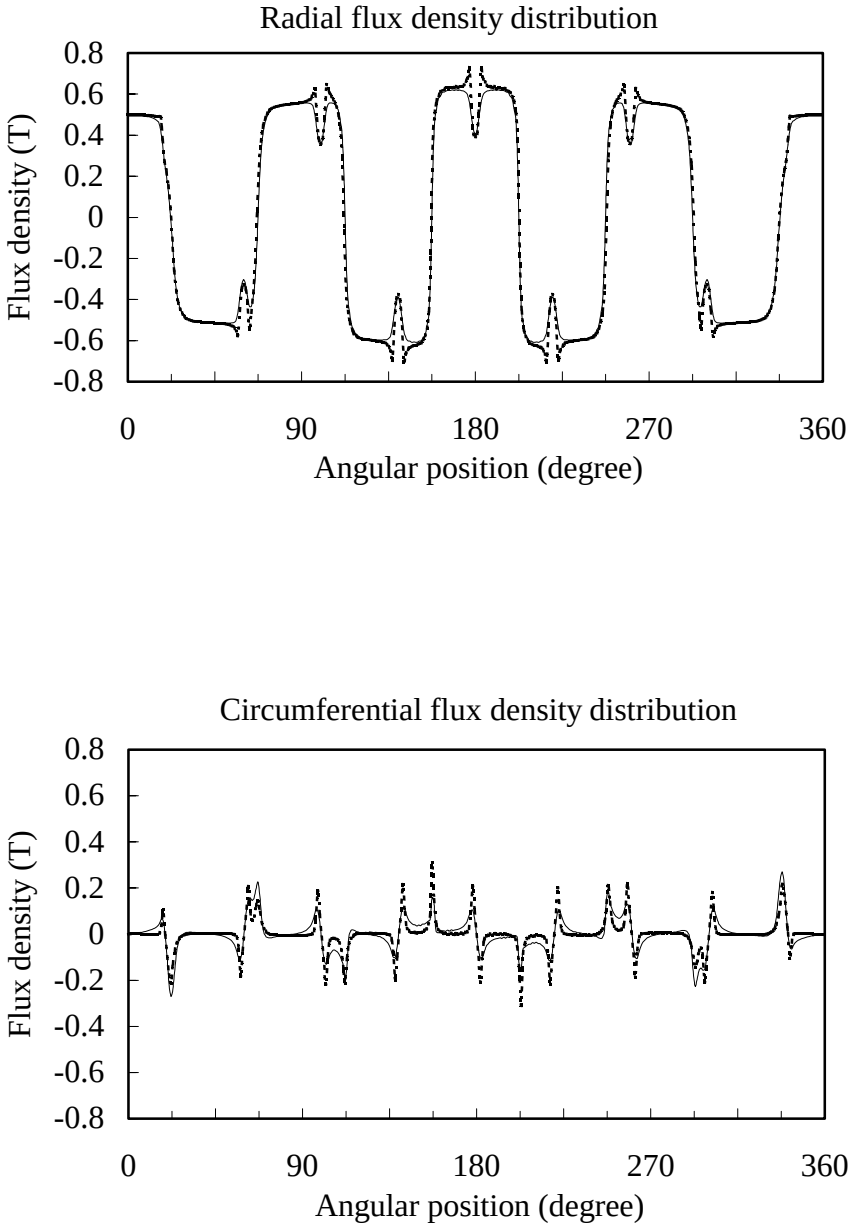

Fig. 6. Flux density distributions in the air gap ($R_s+0.2g$) of motor I with the rotor eccentricity of $\varepsilon=0.5g$. Solid line : analytical results (by perturbation) ; dotted line : FEM results.

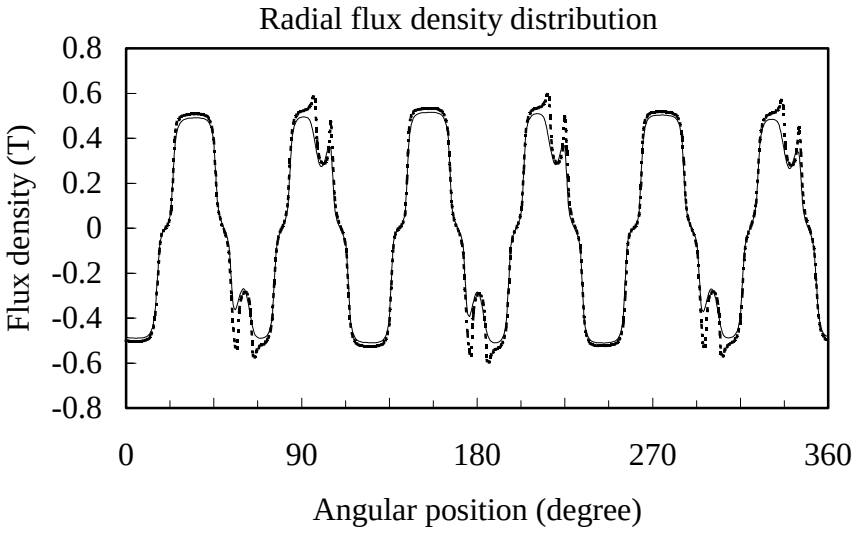

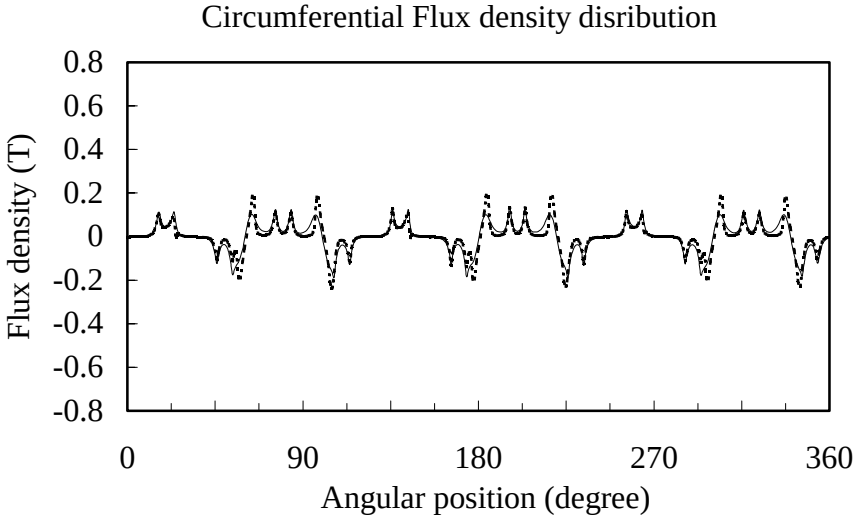

Fig. 7. Flux density distributions in the air gap ($R_s+0.5g$) of motor II with the rotor eccentricity of $\varepsilon=0.1g$ at an instance of $\omega t=14.5^o$ and $\varphi=45^o$. Solid line: analytical results (by perturbation); dotted line: FEM results.

Appendix I. The Integration Constants in Eq. (12) and (13)

$$\hat{A}_{1n}^{0}=\frac{M_n}{1-(np)^2}\frac{\left(\bar{r}_m^{2np}+1\right)\left(\bar{r}_m^{np+1}-1\right)-\left(\bar{r}_m^{2np}-1\right)\left(1+np\bar{r}_m^{np+1}\right)}{\mu_r\left(\bar{r}_m^{2np}+\bar{r}_s^{2np}\right)\left(\bar{r}_m^{2np}+1\right)-\left(\bar{r}_m^{2np}-\bar{r}_s^{2np}\right)\left(\bar{r}_m^{2np}-1\right)}$$

$$\hat{C}_{1nm}^{0}=-\frac{B_{nm}}{\mu_0}\frac{\bar{r}_s^{np+mq+1}\left\{\left(1+\mu_r\right)\bar{r}_m^{2np+2mq}+\left(\mu_r-1\right)\right\}}{\bar{r}_s^{2np+2mq}\left\{\left(1+\mu_r\right)\bar{r}_m^{2np+2mq}+\left(\mu_r-1\right)\right\}-\bar{r}_m^{2np+2mq}\left\{\left(1-\mu_r\right)\bar{r}_m^{2np+2mq}-\left(\mu_r+1\right)\right\}}$$

$$\hat{D}_{1nm}^{0}=-\frac{B_{nm}}{\mu_0}\frac{\bar{r}_s^{np+mq+1}\bar{r}_m^{2np+2mq}\left\{\left(1-\mu_r\right)\bar{r}_m^{2np+2mq}-\left(\mu_r+1\right)\right\}}{\bar{r}_s^{2np+2mq}\left\{\left(1+\mu_r\right)\bar{r}_m^{2np+2mq}+\left(\mu_r-1\right)\right\}-\bar{r}_m^{2np+2mq}\left\{\left(1-\mu_r\right)\bar{r}_m^{2np+2mq}-\left(\mu_r+1\right)\right\}}$$

$$\hat{E}_{1nm}^{0}=-\frac{B_{nm}}{\mu_0}\frac{\bar{r}_s^{np-mq+1}\left\{\left(1+\mu_r\right)\bar{r}_m^{2np-2mq}+\left(\mu_r-1\right)\right\}}{\bar{r}_s^{2np-2mq}\left\{\left(1+\mu_r\right)\bar{r}_m^{2np-2mq}+\left(\mu_r-1\right)\right\}-\bar{r}_m^{2np-2mq}\left\{\left(1-\mu_r\right)\bar{r}_m^{2np-2mq}-\left(\mu_r+1\right)\right\}}$$

$$\hat{F}_{1nm}^{0}=-\frac{B_{nm}}{\mu_0}\frac{\bar{r}_s^{np-mq+1}\bar{r}_m^{2np-2mq}\left\{\left(1-\mu_r\right)\bar{r}_m^{2np-2mq}-\left(\mu_r+1\right)\right\}}{\bar{r}_s^{2np-2mq}\left\{\left(1+\mu_r\right)\bar{r}_m^{2np-2mq}+\left(\mu_r-1\right)\right\}-\bar{r}_m^{2np-2mq}\left\{\left(1-\mu_r\right)\bar{r}_m^{2np-2mq}-\left(\mu_r+1\right)\right\}}$$

where

$$M_n=2\left(\frac{B_r}{\mu_0}\right)\alpha_p\frac{\sin\left(\frac{n\pi\alpha_p}{2}\right)}{\left(\frac{n\pi\alpha_p}{2}\right)}$$

$$B_{nm}=-\mu_0(np)\bar{r}_s^{np-1}\lambda_m\hat{B}_n$$

$$\hat{B}_n=\frac{M_n}{1-(np)^2}\frac{\left(1+np\bar{r}_m^{np+1}\right)\left(\bar{r}_m^{2np}-1\right)-\left(\bar{r}_m^{2np}+1\right)\left(\bar{r}_m^{np+1}-1\right)}{\left(\bar{r}_m^{2np}+\bar{r}_s^{2np}\right)\left(\bar{r}_m^{2np}-1\right)-\mu_r\left(\bar{r}_m^{2np}-\bar{r}_s^{2np}\right)\left(\bar{r}_m^{2np}+1\right)}$$

$$\bar{r}_s=\left(\frac{R_s}{R_r}\right)$$

$$\bar{r}_m=\left(\frac{R_m}{R_r}\right)$$

Appendix II. The Integration Constants in Eq. (51) and (52)

$$\hat{A}_{1n}^{1}=-\frac{(np)^2\,\hat{A}_{1n}^{0}\bar{r}_s^{2np}\left\{(1+\mu_r)\bar{r}_m^{2np+2}-(1-\mu_r)\right\}}{\bar{r}_m^{2np+2}\left\{(1-\mu_r)\bar{r}_m^{2np+2}-(1+\mu_r)\right\}-\bar{r}_m^{2np+2}\left\{(1+\mu_r)\bar{r}_m^{2np+2}-(1-\mu_r)\right\}}$$

$$\hat{B}_{1n}^{1}=-\frac{(np)^2\,\hat{A}_{1n}^{0}\bar{r}_s^{2np}\bar{r}_m^{2np+2}\left\{(1-\mu_r)\bar{r}_m^{2np+2}-(1+\mu_r)\right\}}{\bar{r}_m^{2np+2}\left\{(1-\mu_r)\bar{r}_m^{2np+2}-(1+\mu_r)\right\}-\bar{r}_m^{2np+2}\left\{(1+\mu_r)\bar{r}_m^{2np+2}-(1-\mu_r)\right\}}$$

$$\hat{C}_{1n}^{1}=-\frac{(np)^2\,\hat{A}_{1n}^{0}\bar{r}_s^{2np}\left\{(1+\mu_r)\bar{r}_m^{2np+2}-(1-\mu_r)\right\}}{\bar{r}_m^{2np-2}\left\{(1-\mu_r)\bar{r}_m^{2np-2}-(1+\mu_r)\right\}-\bar{r}_m^{2np-2}\left\{(1+\mu_r)\bar{r}_m^{2np+2}-(1-\mu_r)\right\}}$$

$$\hat{D}_{1n}^{1}=-\frac{(np)^2\,\hat{A}_{1n}^{0}\bar{r}_s^{2np}\bar{r}_m^{2np}\left\{(1-\mu_r)\bar{r}_m^{2np-2}-(1+\mu_r)\right\}}{\bar{r}_m^{2np-2}\left\{(1-\mu_r)\bar{r}_m^{2np-2}-(1+\mu_r)\right\}-\bar{r}_m^{2np-2}\left\{(1+\mu_r)\bar{r}_m^{2np+2}-(1-\mu_r)\right\}}$$

$$\hat{E}_{1n}^{1}=-\frac{T_1\cdot\left\{(1+\mu_r)\bar{r}_m^{2np+2mq-2}-(1-\mu_r)\right\}}{\bar{r}_m^{2np+2mq-2}\left\{(1-\mu_r)\bar{r}_m^{2np+2mq-2}-(1+\mu_r)\right\}-\bar{r}_s^{2np+2mq-2}\left\{(1+\mu_r)\bar{r}_m^{2np+2mq-2}-(1-\mu_r)\right\}}$$

$$\hat{F}_{1n}^{1}=-\frac{T_1\cdot\bar{r}_m^{2np+2mq-2}\left\{(1-\mu_r)\bar{r}_m^{2np+2mq-2}-(1+\mu_r)\right\}}{\bar{r}_m^{2np+2mq-2}\left\{(1-\mu_r)\bar{r}_m^{2np+2mq-2}-(1+\mu_r)\right\}-\bar{r}_s^{2np+2mq-2}\left\{(1+\mu_r)\bar{r}_m^{2np+2mq-2}-(1-\mu_r)\right\}}$$

$$\hat{G}_{1n}^{1}=-\frac{T_2\cdot\left\{(1+\mu_r)\bar{r}_m^{2np-2mq-2}-(1-\mu_r)\right\}}{\bar{r}_m^{2np-2mq-2}\left\{(1-\mu_r)\bar{r}_m^{2np-2mq+2}-(1+\mu_r)\right\}-\bar{r}_s^{2np-2mq-2}\left\{(1+\mu_r)\bar{r}_m^{2np-2mq-2}-(1-\mu_r)\right\}}$$

$$\hat{H}_{1n}^{1}=-\frac{T_2\cdot\bar{r}_m^{2np-2mq-2}\left\{(1-\mu_r)\bar{r}_m^{2np-2mq-2}-(1+\mu_r)\right\}}{\bar{r}_m^{2np-2mq-2}\left\{(1-\mu_r)\bar{r}_m^{2np-2mq+2}-(1+\mu_r)\right\}-\bar{r}_s^{2np-2mq-2}\left\{(1+\mu_r)\bar{r}_m^{2np-2mq-2}-(1-\mu_r)\right\}}$$

$$\hat{I}_{1n}^{1}=-\frac{T_3\cdot\left\{(1+\mu_r)\bar{r}_m^{2np+2mq+2}-(1-\mu_r)\right\}}{\bar{r}_m^{2np+2mq+2}\left\{(1-\mu_r)\bar{r}_m^{2np+2mq+2}-(1+\mu_r)\right\}-\bar{r}_s^{2np+2mq+2}\left\{(1+\mu_r)\bar{r}_m^{2np+2mq+2}-(1-\mu_r)\right\}}$$

$$\hat{J}_{1n}^{1}=-\frac{T_3\cdot\bar{r}_m^{2np+2mq+2}\left\{(1-\mu_r)\bar{r}_m^{2np+2mq+2}-(1+\mu_r)\right\}}{\bar{r}_m^{2np+2mq+2}\left\{(1-\mu_r)\bar{r}_m^{2np+2mq+2}-(1+\mu_r)\right\}-\bar{r}_s^{2np+2mq+2}\left\{(1+\mu_r)\bar{r}_m^{2np+2mq+2}-(1-\mu_r)\right\}}$$

$$\hat{K}_{1n}^{1}=-\frac{T_4\cdot\left\{\left(1+\mu_r\right)\bar{r}_m^{2np-2mq+2}-\left(1-\mu_r\right)\right\}}{\bar{r}_m^{2np-2mq+2}\left\{\left(1-\mu_r\right)\bar{r}_m^{2np-2mq+2}-\left(1+\mu_r\right)\right\}-\bar{r}_s^{2np-2mq+2}\left\{\left(1+\mu_r\right)\bar{r}_m^{2np-2mq+2}-\left(1-\mu_r\right)\right\}}$$

$$\hat{L}_{1n}^{1}=-\frac{T_4\cdot\bar{r}_m^{2np-2mq+2}\left\{\left(1-\mu_r\right)\bar{r}_m^{2np-2mq+2}-\left(1+\mu_r\right)\right\}}{\bar{r}_m^{2np-2mq+2}\left\{\left(1-\mu_r\right)\bar{r}_m^{2np-2mq+2}-\left(1+\mu_r\right)\right\}-\bar{r}_s^{2np-2mq+2}\left\{\left(1+\mu_r\right)\bar{r}_m^{2np-2mq+2}-\left(1-\mu_r\right)\right\}}$$

where

$$T_1=\frac{1}{2}\left\{\left(np+mq-1\right)\hat{C}_{1nm}^{0}\bar{r}_s^{2np+2mq-2}+\left(np+mq+1\right)\hat{D}_{1nm}^{0}\bar{r}_s^{-2}\right\}-\frac{R_s}{\mu_0}X_{nm}\lambda_m\bar{r}_s^{np+mq-1}$$

$$T_2=\frac{1}{2}\left\{\left(np-mq-1\right)\hat{E}_{1nm}^{0}\bar{r}_s^{2np-2mq-2}+\left(np-mq+1\right)\hat{F}_{1nm}^{0}\bar{r}_s^{-2}\right\}-\frac{R_s}{\mu_0}X_{nm}\lambda_m\bar{r}_s^{np+mq-1}$$

$$T_3=\frac{1}{2}\left\{\left(np+mq-1\right)\hat{C}_{1nm}^{0}\bar{r}_s^{2np+2mq}+\left(np+mq+1\right)\hat{D}_{1nm}^{0}\right\}-\frac{R_s}{\mu_0}Z_{nm}\lambda_m\bar{r}_s^{np+mq+1}$$

$$T_4=\frac{1}{2}\left\{\left(np-mq-1\right)\hat{E}_{1nm}^{0}\bar{r}_s^{2np-2mq}+\left(np-mq+1\right)\hat{F}_{1nm}^{0}\right\}-\frac{R_s}{\mu_0}Z_{nm}\lambda_m\bar{r}_s^{np-mq+1}$$

APPENDIX III. The Design Parameters of Motors for Examples.

Design Parameter		MOTOR I		MOTOR II	
Stator Radius	R_s	9.725	(mm)	10.64	(mm)
Magnet thickness	h_m	1.0	(mm)	0.8	(mm)
Air gap length	g	0.25	(mm)	0.25	(mm)
Pole number	$2p$	8		12	
PM dead angle		0	(degree)	8	(degree)
Slot opening angle		5	(degree)	8	(degree)
Magnet remanence	B_r	0.71	(T)	0.71	(T)
Relative permeance	μ_r	1.26		1.26	
Magnetization direction		Radial		Radial	